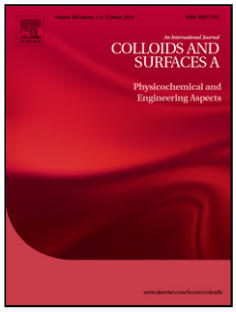

Title: Polyacrylic acid-coated iron oxide magnetic nanoparticles: the polymer molecular weight influence

Authors: Laura M. Sanchez, Daniel A. Martin, Vera A. Alvarez, Jimena S. Gonzalez

PII: S0927-7757(18)30063-3
DOI: https://doi.org/10.1016/j.colsurfa.2018.01.050
Reference: COLSUA 22245

To appear in: *Colloids and Surfaces A: Physicochem. Eng. Aspects*

Received date: 12-12-2017
Revised date: 19-1-2018
Accepted date: 26-1-2018

Please cite this article as: Sanchez LM, Martin DA, Alvarez VA, Gonzalez JS, Polyacrylic acid-coated iron oxide magnetic nanoparticles: the polymer molecular weight influence, *Colloids and Surfaces A: Physicochemical and Engineering Aspects* (2010), https://doi.org/10.1016/j.colsurfa.2018.01.050

Polyacrylic acid-coated iron oxide magnetic nanoparticles: the polymer molecular weight influence.

Laura M. Sanchez[1,*], Daniel A. Martin[2], Vera A. Alvarez[1] and Jimena S. Gonzalez[1]

[1]Materiales Compuestos Termoplásticos, Instituto de Investigaciones en Ciencia y Tecnología de Materiales (INTEMA), CONICET - Universidad Nacional de Mar del Plata (UNMdP). Av. Colón 10890, Mar del Plata, 7600, Argentina.

[2]Instituto de Investigaciones Físicas de Mar del Plata (IFIMAR-CONICET) - Departamento de Física, FCEyN, Universidad Nacional de Mar del Plata (UNMdP). Dean Funes 3350, Mar del Plata, 7600, Argentina.

*Corresponding author: Dr. Laura Mabel Sanchez. Phone Nº: (+54 223) 6260600; e-mail: lsanchez@mdp.edu.ar

Graphical abstract

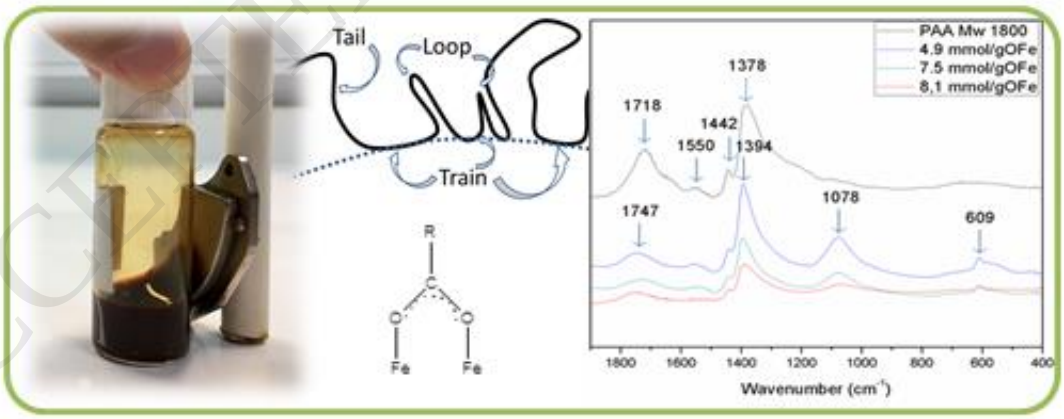

Abstract

Magnetic nanoparticles (MNPs), in particular, magnetic iron oxide-based nanoparticles were found to be useful as catalysts and as devices for data storage, environmental remediation and several biomedical applications, due to their excellent properties, such as biocompatibility and high magnetic moment. Polyacrylic acid (PAA) is a weak polyelectrolyte that can be used to stabilize the MNPs. To the best of our knowledge, the influence of PAA molecular weight and PAA concentration over the magnetic and structural properties of iron oxide nanoparticles has not been previously reported. The aim of this paper is to describe the differences evidenced in the properties of different magnetic materials by using PAA for iron oxides stabilization by one-pot coprecipitation synthesis. Iron oxide-based magnetic nanoparticles stabilized by polyacrylic acid (PAA) polymers were efficiently prepared and exhaustively characterized. The influence on the employment of two different low PAA molecular weights, Mw 1800 g/mol and 5000 g/mol, in three different iron salts: PAA ratios was analyzed. In summary, the main results showed that: for a certain PAA reactor feed higher oligomer quantities are present in MNPs as higher is the involved molecular weight of the polymeric chain; when molecular weight raises the contribution of loops and tails also does it, allowing having higher polymer contents. For both PAA's Mw employed as the adsorbed PAA increases particles hydrodynamic diameters decreases, and their distribution becomes narrower; the PAA adsorbs onto iron oxides by chemisorption (the most probable interaction is the bidentate bridging). For the studied cases z potential values depend much more on the PAA's quantity adsorbed onto the iron oxides than on the PAA's Mw. MNPs are superparamagnetic and choosing the right shape of particle distribution is not central for getting estimates of the magnetization saturation, the average particle diameter and its standard deviation, while better fits are found with Normal and Log-Normal particle size distributions.

Keywords: Magnetic nanoparticles, polyacrylic acid, magnetite.

1. Introduction

From some decades up to now, nanomaterials are being widely prepared and employed for a variety of applications. Magnetic nanoparticles (MNPs) were found to be useful as catalysts and as devices for both data storage and environmental remediation, among many other possibilities [1]. They are also employed for several biomedical applications, such as drug delivery systems [2] and contrast agents for MRI [3]. In particular, the preparation and application of magnetic iron oxide-based nanoparticles as biocatalysts [4], hyperthermia devices [5], therapeutic agents for cancer treatments and magnetic media have been reported [6] due to excellent properties, such as biocompatibility and high magnetic moment [7].

As a result of their small size, MNPs agglomeration is a well-known fact. Thus, many efforts have been conducted to achieve the necessary and desired nanoparticles stability on the corresponding ferrofluids suspensions. One of the most widely employed strategy consists on preparing the MNPs through coprecipitation from iron salts, in presence of a stabilizing agent. The aqueous coprecipitation method of MNPs synthesis produces biocompatible iron oxide NPs of non-toxical reagents at lower temperatures than other methods, such as thermal decomposition preparation process. However, a broad NPs size distribution and poor repeatability was reported for this method [8].

Among a number of possible stabilizing agents, some carboxylated compounds, such as citric, polyacrylic, poly (acrylic-co-maleic), humic and gallic acids have been employed [9,10]. It is important to remark that polyelectrolytes not only stabilize the particles, but also they can flocculate them. According to several reports, flocculation takes place when polymers of high molecular weight are used because two or more colloidal particles could be bound to each other. This process is commonly named ‘bonding’ [11,12]. The agglomeration and particle size of composite nanoparticles are influenced by the type of the surfactant employed and its concentration [13].Among these surface modification substances, polyacrylic acid (PAA) has been used to stabilize MNPs by providing electrostatic and steric repulsion against particle aggregation [14]. The synthesis of PAA-Coated Magnetite Nanoparticles has been reported following thermal decomposition route [15] or initiated atom transfer radical polymerization [14].

PAA is a weak polyelectrolyte with a variable degree of dissociation, which depends on the solution pH and ionic strength. Moreover, PAA is a water-soluble polymer with a high binding capacity. It also has a high density of reactive functional groups, which provides a strong

linkage between the iron oxide and biomolecules, making it very attractive for biomedical applications [16].

The final product dependance on pH, reagent, surfactant and iron salt ratio has already been studied. Also, the mechanisms of nanoparticles formation over the magneto-structural properties has been reported [17]. To the best of our knowledge, the influence of PAA molecular weight and PAA concentration over the magnetic and structural properties of iron oxide nanoparticles has not been previously reported. The aim of this paper is to describe the differences evidenced in the properties of different magnetic materials by using PAA for iron oxides stabilization by one-pot synthesis. To this purpose, the influence on the employment of two different low PAA molecular weights, Mw 1800 g/mol and 5000 g/mol, under three different iron salts/ PAA ratios was exhaustively analyzed. Studies of the final products were conducted *via* Fourier Transformed Infrared Spectroscopy (FTIR), X-Ray diffraction (XRD), Dynamic light scattering (DLS), z-potential, Thermogravimetric analysis (TGA) transmission electron microscopy (TEM) and magnetic measurements. The influence of PAA molecular weights on the final oligomer quantities present on MNPs for a certain reactor feed, on the MNPs hydrodynamic diameter and their sizes distribution and on z-potential was determined and explained.

From FTIR studies, the possible interactions between the polymeric chains and the iron oxides, both present in the MNPs were elucidated and described. From magnetic measurements results, superparamagnetic response was characterized. It was shown that most relevant parameters are roughly independent on proposed particle size distributions. The results obtained by XRD and TEM were compared and related with those estimated from magnetization measurements.

2. Materials and methods

2.1-Materials

For iron oxide MNPs preparation, two different iron salts were used as starting materials: $FeSO_4.7H_2O$ and $FeCl_3.6H_2O$ (both from Cicarelli Laboratory, Argentina). Furthermore, two PAA were employed: Mw 1800 g/mol and 5000 g/mol both purchased from Polysciences. Other reactants were also incorporated: NH_4OH (Biopack, Argentina), HCl (Biopack, Argentina), and bidistilled water.

2.2-Methods

PAA-coated MNPs were prepared through coprecipitation method, according to Lin and collaborators [18]. Briefly, 4.75 g of $FeCl_3.6H_2O$ and 2.45 g of $FeSO_4.7H_2O$ were dissolved in 80 mL of milli-Q water at 60 °C, under N_2 atmosphere. Then, PAA was added to the system (0.32, 0.49 and 0.63 g) and vigorous stirring was maintained for 30 min. After this, 10 mL of NH_4OH were quickly added, resulting in a color change from orange to black.

By following the above-mentioned procedure six different ferrofluids were thus obtained: three different PAA concentrations for each Mw employed. Each of them was purified by dialysis (until pH and conductivity reached those corresponding to distilled water) and then they were exhaustively characterized. In order to determine the quantitative and qualitative compositions of the samples, thermo gravimetric (TGA), X-ray diffraction analysis (XRD) and FT-IR measurements for dry MNPs were done. For this, samples were dried in an oven at 45 °C until constant weight. TGA was conducted in a TA-Q500 equipment from room temperature to 800°C under N_2 atmosphere at a heating rate of 10°C/min. In the case of XRD, measurements of dried samples took place in an Analytical Expert Instrument for 2θ values from 10 to 65 degrees at a rate of 2°/min. For this, monochromatic Cu-Kα radiation was employed. FT-IR measurements were done in a Thermo Scientific Nicolet 6700 spectrometer, employing a resolution of 4 cm^{-1}. Measurements were carried out in attenuated total reflectance modes (smart Orbit ATR accessory) from 400 to 4000 cm^{-1}.

To know well MNPs sizes, sizes distribution, morphology and superficial charges, dynamic light scattering (DLS) and transmission electron microscopy (TEM) measurements were done. The hydrodynamic particle diameters, size distribution and zeta potential were measured at room temperature by DLS in a Malvern Zetasizer equipment. Dispersions of the dried MNPs were prepared in ethanol-water solutions (50%-50%, suspensions concentrations were 1 mg/10 mL)

and water (suspensions concentrations were 0.5 mg/10 mL) for triplicate size distribution and zeta potential measurements, respectively. For zeta potential determinations the Smoluchowski equation was used. Some of the prepared MNPs were observed by TEM to examine the respective morphologies in a JEOL100-CX II-Japan (CRIBABB –CCT - Bahía Blanca, Argentina). To this, MNPs suspensions were prepared by using ethanol-water solutions (50%-50%).

Finally, measurements of magnetization of the MNPs were also done. For this, SQUID magnetometry was used. Approximately 60 mg of the suspensions were measured at room temperature as a function of the applied magnetic field between from -20 kOe to 20 kOe.

3. Results and Discussion

3.1-Ferrofluids preparation

Six different ferrofluids were successfully prepared through coprecipitation method from iron salts, each of them obtained in the presence of different quantities of two different PAA's Mw, 1800g/mol and 5000g/mol. All systems were stable showing iron oxides nanoparticles suspended in aqueous medium during months. The first approximation to know if MNPs present magnetic response was to put them under the presence of a permanent magnet, and it was observed that their response was positive (Figure 1). The ferrofluids concentration on MNPs was determined gravimetrically.

Figure 1. MNPs response under the presence of a permanent magnet.

3.2-Quantitative composition analysis

In order to determine the iron oxide/PAA ratio in MNPs thermo gravimetric analysis were conducted. A typical thermogram is shown in Figure 2.

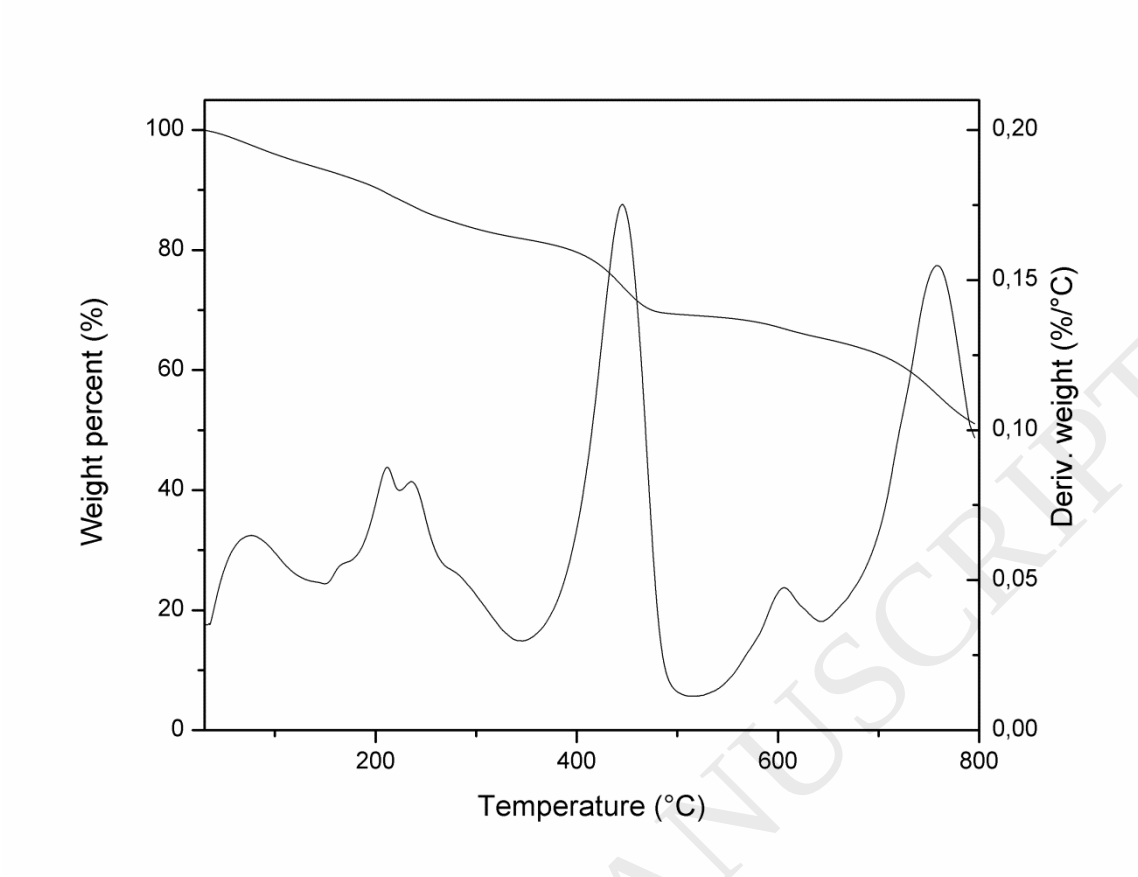

Figure 2. Thermogram obtained for one of the MNPs prepared.

The different events responsible of each weight loss could be identified, as have been described in previous reports [18–20]. The initial weight loss (around 200-250 °C) is associated with dehydration and decarboxylation of the PAA oligomers. Then, the complete degradation of PAA oligomers could be considered done before 500 °C. Finally, at ~700-750 °C and under N_2 atmosphere the deoxidization of iron oxides takes place. The final value at 800 °C was taken as total Iron Oxides mass in the sample.

The obtained data for the six different MNPs prepared is presented in Figure 3. Results are expressed as PAA in MNPs (number of acrylic acid monomers per 1 g of iron oxides, considering that the molar mass of acrylic acid (AA) monomers is 72 Da) as a function of the PAA amount added to the initial preparation mixture (expressed as number of acrylic acid monomers per 1 L of solution, considering the previous mentioned molar mass of AA).

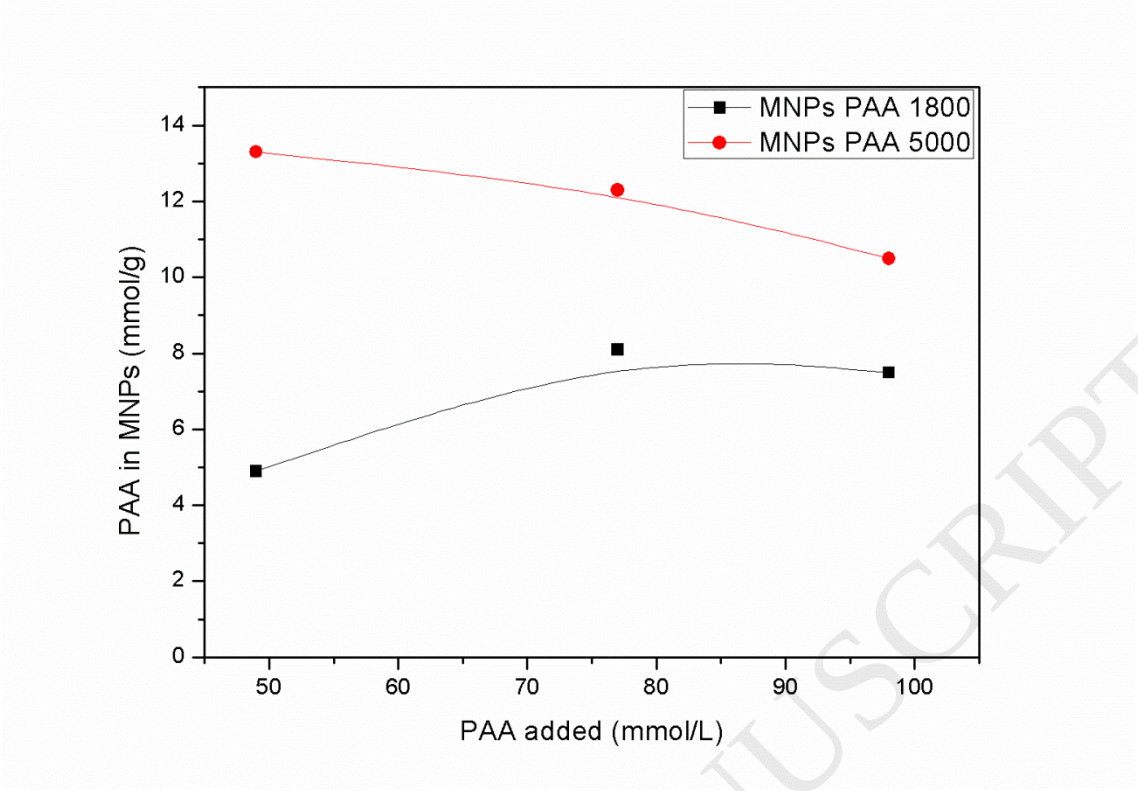

Figure 3. PAA content in MNPs as a function of the PAA added in the initial preparation system.

From Figure 3 it can be observed that, for a certain PAA reactor feed, higher oligomer quantities are present in MNPs as higher is the involved molecular weight of the polymeric chain. This effect could be associated with the adopted conformations: when molecular weight raises the contribution of loops and tails (Figure 4) also does, allowing having higher polymer contents. This fact has been reported by several authors that studied the adsorption of polymeric chains onto different oxides [11,12,21,22].

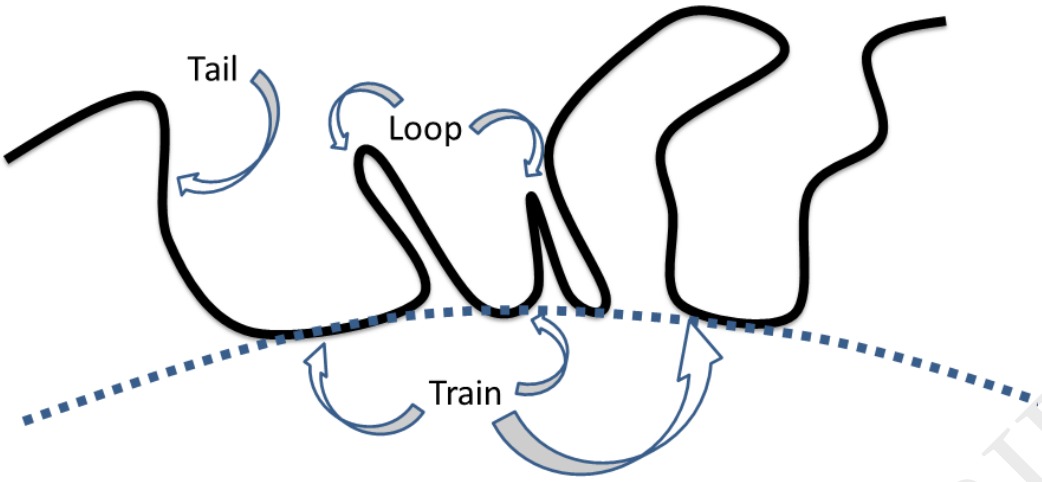

Figure 4. Schematic representation of tails, loops and trains in an adsorbed polymer.

On the other side, the polymer concentration also has an influence on the adopted conformation. In general, when polymer concentration rises, it is possible that chains adopt a perpendicular arrangement to the solid's surface, allowing the presence of a higher quantity of free sites on this surface [23]. This could explain why higher concentration of the lower molecular weight of PAA in the reactor feed results in higher PAA content on MNPs.

3.3-Qualitative composition analysis

To determine the nature of the iron oxide/iron oxides mixture present in the prepared MNPs, their XRD analysis was conducted. Obtained results are shown in Figure 5.

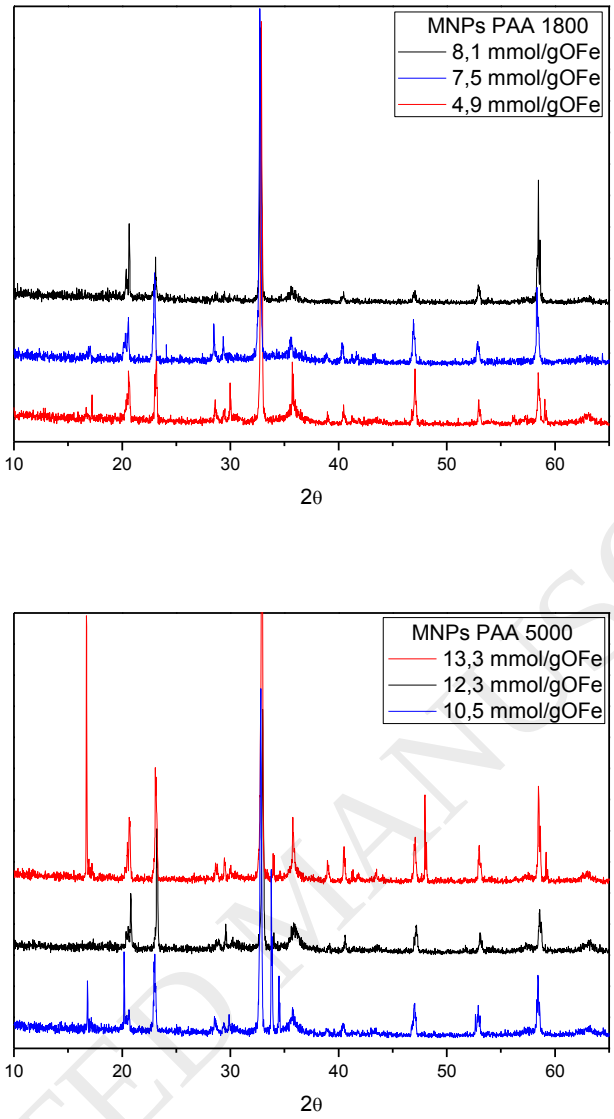

Figure 5. XRD results for MNPs prepared with two different PAA's Mw.

From Figure 5 analysis and later comparison with literature, it can be seen that all samples have the characteristic diffraction peaks for PAA-coated magnetite nanoparticles: 2θ= 30.2°, 35.7°, 43.4°, 53.7°, 57.4°, and 62.9° corresponding to Fe_3O_4 nanoparticles and 2θ= 20° for PAA [18]. Besides, other diffraction peaks are present and they indicate the presence of an iron oxides mixture. For example, the very intense peak at 2θ= 32.8 ° indicates the presence of Fe_2O_3 crystal. The presence of an iron oxides mixture in the ferrofluid could be due to the partial oxidation of some Fe^{+2} to Fe^{+3} at the initial pH condition of synthesis (pH ~3).

In the PAA-coated MNPs system there are several interaction possibilities between the polymeric chains and the iron oxides. According to the bibliography, the Fe atoms exposed on the surface of the iron oxides would adsorb COO^- groups of the PAA. There are three possibilities of coordination between COO^- groups and Fe atoms: unidentate, bidentate and bridging (Structures I, II and III, Figure 6) [24]. Furthermore, the superficial oxygen atoms of the iron oxides would adsorb H^+. Thus, the OH/OH_2^+ species present on the surface also could react with the residual carboxylic/carboxylate groups of the PAA giving structure IV from Figure 6 [18,25].

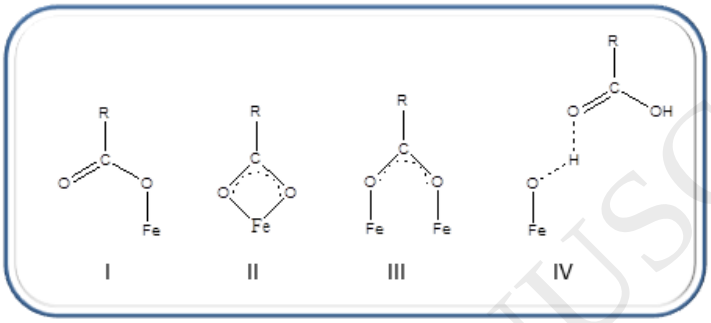

Figure 6. Possible interactions between the polymeric chains and the iron oxides both present in the MNPs.

Since interactions could be inferred from data present on FTIR spectra, the corresponding measurements and analysis were conducted (Figure 7). Both employed PAA present a -C=O band at 1718 cm^{-1} corresponding to carboxylates of acid species, while in the MNPs spectra, this band is displaced to 1747 cm^{-1} indicating the possible formation of some ester linkages [10]. The band at 1550 cm^{-1} is typical for asymmetrical $–COO^-$ stretching, and it is weakly present in almost the same position on both reactant and MNPs samples. In the case of $–CH_2$ scissoring vibrations band at 1442 cm^{-1}, it is present in PAA sample and it remains unchanged for all MNPs spectra. This fact possibly indicates that the polymer adsorption takes place more in loops than in trains [25].

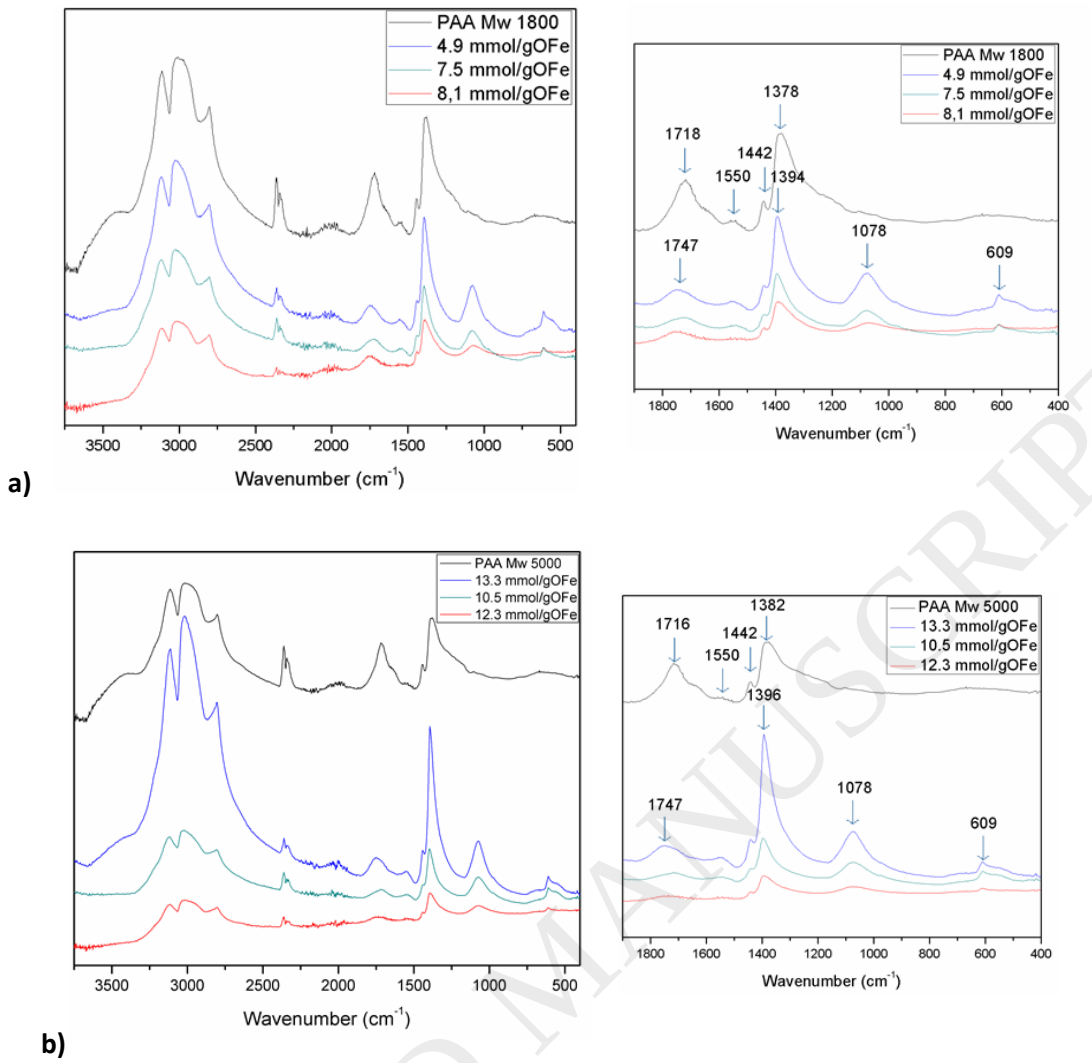

Figure 7. FTIR spectra for MNPs prepared with two different PAA's Mw: a) PAA Mw 1800; b) PAA Mw 5000.

Continuing with the spectra analysis, the symmetrical $–COO^-$ stretching present in 1378/1382 cm^{-1} for PAA samples shifts to approximately 1394/1396 cm^{-1} for MNPs ones. Those displacements of sharp bands to higher wavenumbers indicate that there is an interaction between the PAA functional groups and the iron oxides surface. The 1078 and 609 cm^{-1} signals present in all MNPs spectra correspond to surface –OH groups and Fe-O bands from iron oxides, respectively [25]. Depending on the iron oxide closest environment, the Fe-O band has been observed at 557, 563, 578 and 590 cm^{-1} [25–27].

The absence of the –C=O band at 1650 cm^{-1} indicates that interactions takes place by some kind of bidentate structure (structures II and III, Figure 6). According to literature, it is possible

to infer the specific bidentate conformation by analyzing the carboxylate bands separation between asymmetrical and symmetrical stretches according to:

$$\Delta\nu = (\nu_{asym} - \nu_{sym}) \qquad \text{[Equation 2]}$$

Thus, the obtained Δν value must be compared with the corresponding Δν of the carboxylate salt [28]. For all MNPs, samples Δν values are similar to $\Delta\nu_{(salt)}$ (160 ± 4 cm^{-1}), which indicates that the most probable interaction is the bidentate bridging (structure III, Figure 6). Since the symmetrical $–COO^-$ stretching band is very sharp, the involved bonds must be very similar. All this evidence seems to indicate that the PAA adsorbs onto iron oxides by chemisorption.

3.4-Morphology, size and superficial charges analysis

From XRD results, the crystallite size of the Fe_3O_4 was calculated. To this, from Figure 5 the 35.7º characteristic peak of magnetite was employed to determine full width at half maximum (β). Then, the Debye-Scherrer equation was employed (Equation 1) [29]:

$$D = \frac{0.9\lambda}{\beta\cos\theta} \qquad \text{[Equation 1]}$$

where:

D= Average crystallite size (A);

λ= wavelength of x-rays;

θ= Bragg diffraction angle;

β= full width at half maximum of the considered peak (radians).

All calculated crystallite sizes were of approximately 11-13 nm for MNPs prepared with PAA's Mw 1800 and 9 nm for those prepared employing PAA's Mw 5000. The obtained sizes are slightly bigger than the crystallite sizes obtained for Fe_3O_4 obtained without PAA in the reactor (8.3 nm [18]).

Hydrodynamic particles sizes, its distribution and also their zeta potentials were determined through dynamic light scattering. The obtained results are shown in Figure 8. According to them, for both PAA's Mw employed as the adsorbed PAA increases particles sizes decreases and their distribution becomes narrower. This result is in accordance to previous reports for

PAA-coated magnetite nanoparticles [18]. Furthermore, the obtained polydispersity values were around 0.35 ± 0.07, indicating that samples are moderately polydisperse.

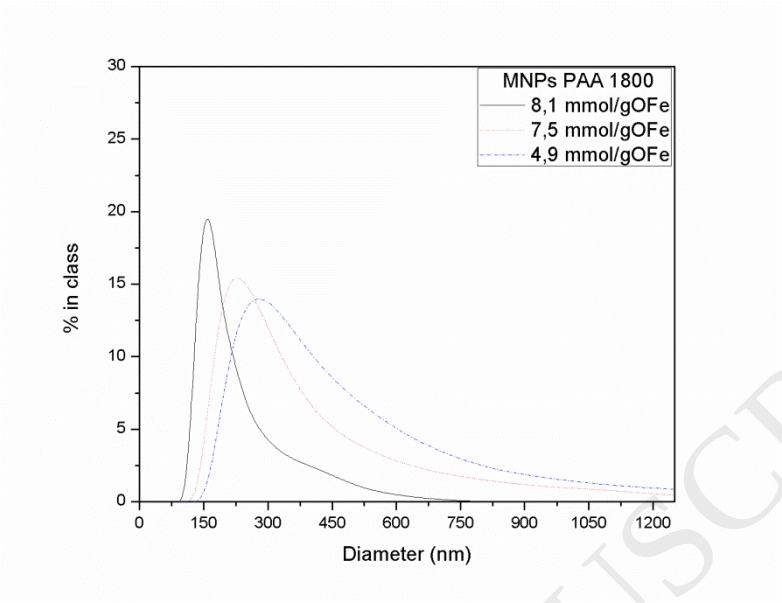

a)

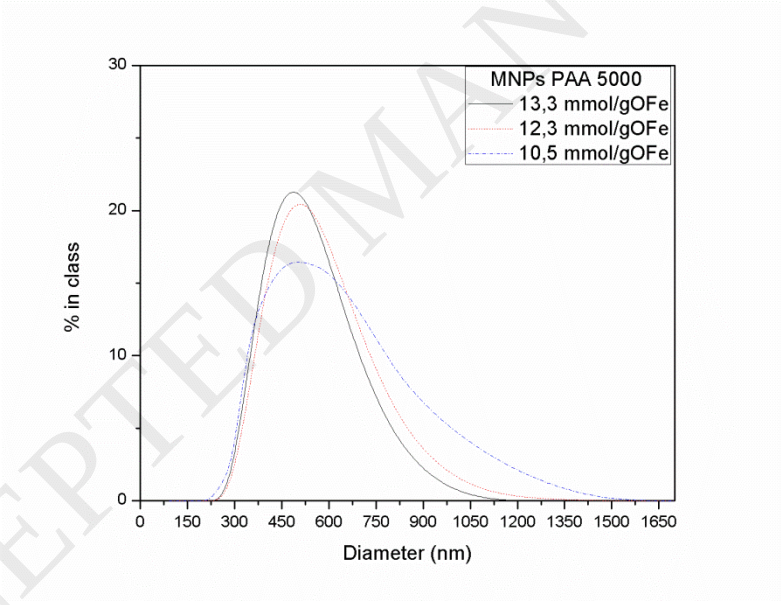

b)

Figure 8. MNPs sizes distribution determined by dynamic light scattering, a) PAA Mw 1800; b) PAA Mw 5000.

It is important to remark that, for a certain PAA-adsorbed amount, the hydrodynamic diameter increases with the increase on PAA's Mw. This fact could be associated with their adopted conformations: when molecular weight raises the contribution of loops and tails also does, and this could allow MNPs to become bigger.

Regarding to z potential of the prepared MNPs, in Figure 9 results are represented. For all samples high negative z potential values were obtained: MNPs have very strong negative charges that provide stabilization through electrostatic repulsion. According to literature, nearby z potential values were obtained for similar MNPs systems [18,30].

Apparently, for the studied cases, z potential values depend much more on the PAA's quantity adsorbed onto the iron oxides than on the PAA's Mw, as if z potential values only depend on the total amount of negative charges.

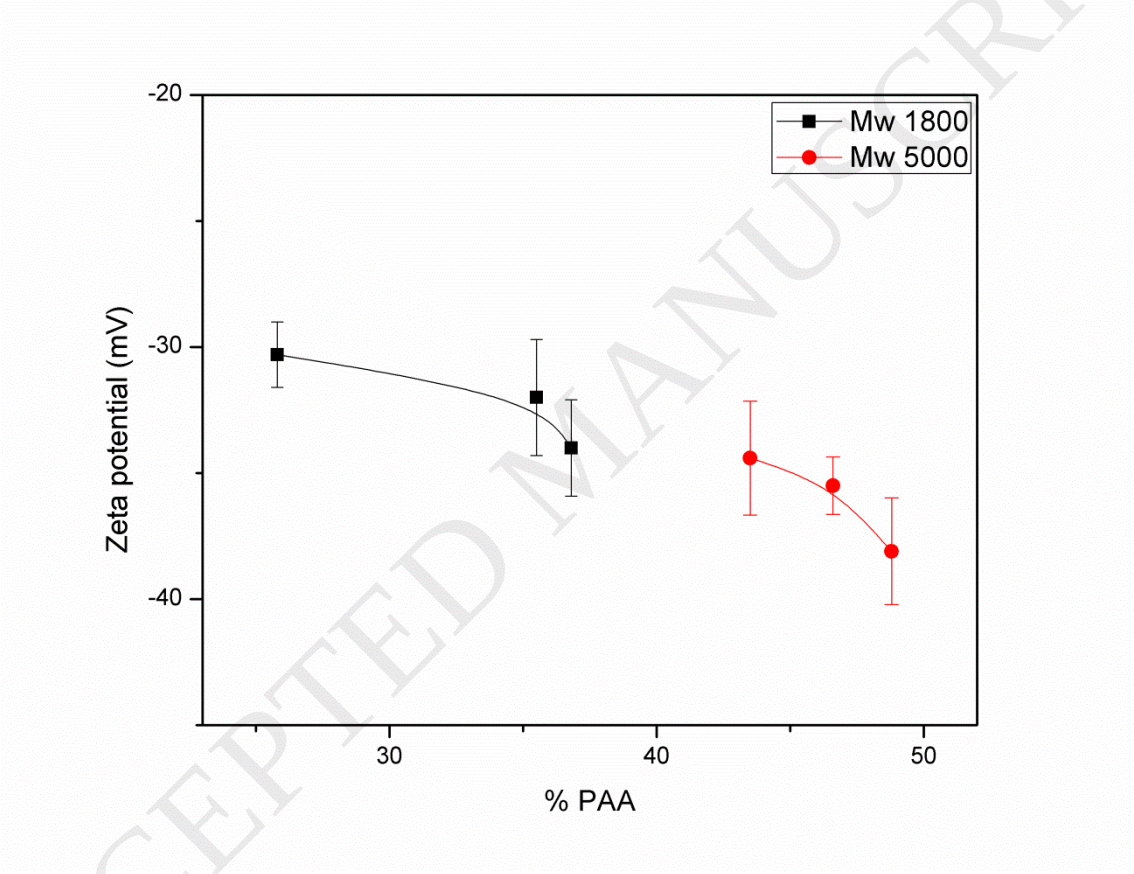

Figure 9. MNPs z potential values as a function of PAA contents for two different Mw. % of PAA refers to the PAA content in the MNPs (i.e. grams of PAA per gram of nanoparticle).

Through transmission electron microscopy images of two samples of the prepared MNPs were obtained (Figure 10).

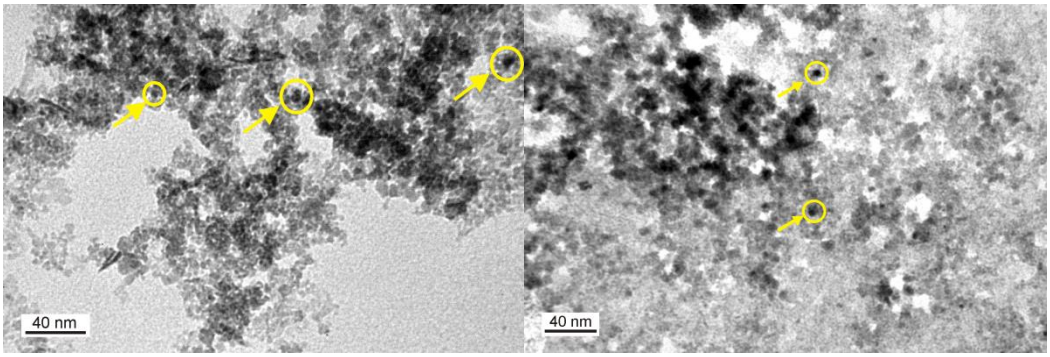

Figure 10. TEM images obtained for a) PAA Mw 1800 8.1 mmol AA/gOFe; b) PAA Mw 5000 12.3 mmol AA/gOFe.

By processing the obtained micrographs with software program, MNPs corresponding sizes were estimated (Figure 11). Furthermore, as it was done previously for DLS results, here it can also be inferred that a higher PAA content conducts to narrower sizes distribution.

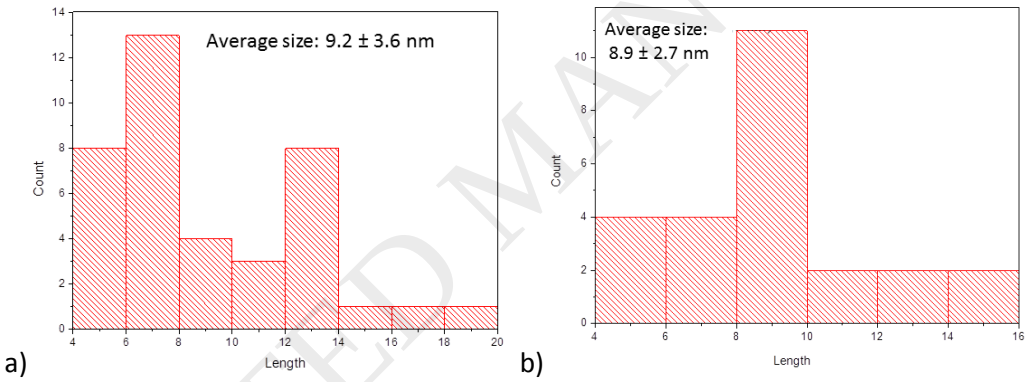

a) b)

Figure 11. Histograms obtained from TEM images for a) PAA Mw 1800 8.1 mmol AA/gOFe; b) PAA Mw 5000 12.3 mmol AA/gOFe.

3.5-Magnetization analysis

The magnetization obtained data were appropriately plotted and fitted. The magnetic response per gram of oxide as a function of magnetic field for one of the samples is shown in Figure 12. An intense nonlinear response was obtained, and the same holds for all our samples.

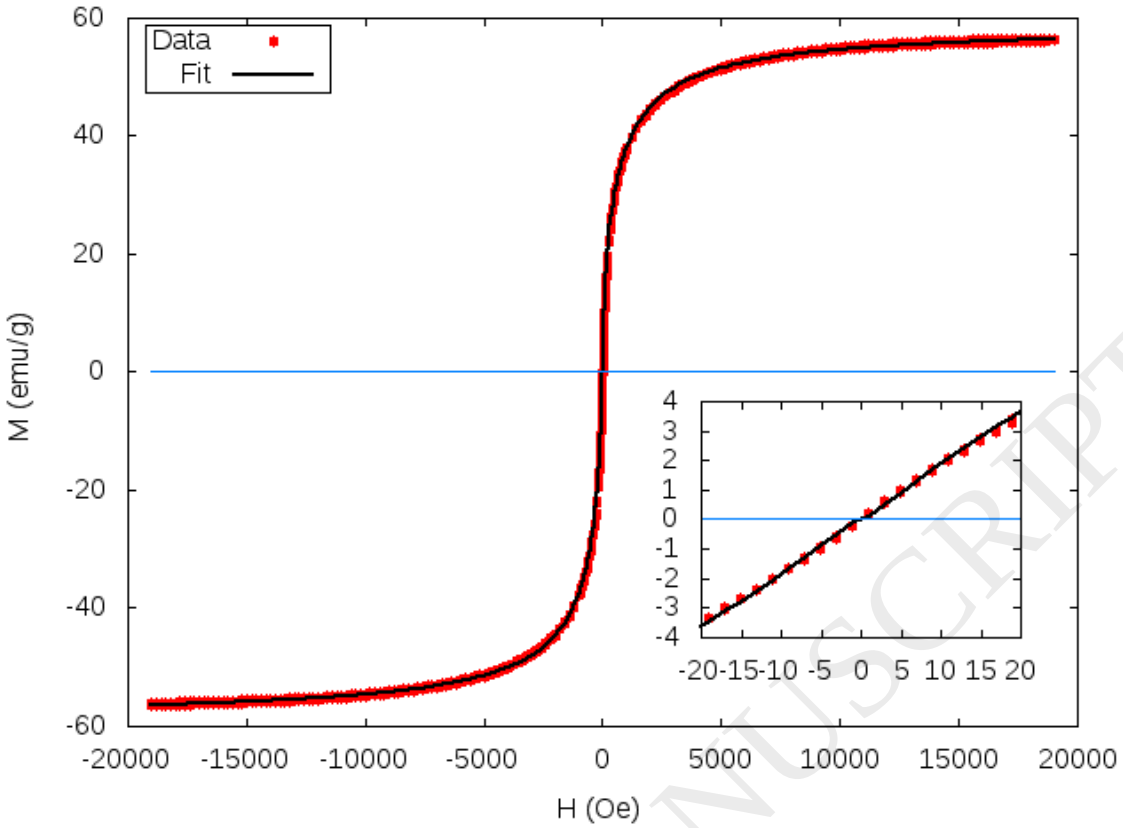

Figure 12. Nonlinear magnetization per gram of oxide as a function of applied magnetic field for one of the MNPs prepared. A fit of the data is also shown. Inset: detail of magnetization curve for small values of H

It was found that coercivity fields, *Hc*, and remanent magnetization *Mr*, where both smaller than measure error. In order to estimate them, low H results were fitted with straight lines (two for each sample). From the difference of these lines, *Hc* values were estimated: about 0.1 Oe for all cases. Remanent magnetization, *Mr*, is also very low for each of the analyzed samples: about 0.01 emu per gram of oxide. Lin and coworkers have shown very similar results for both *Hc* and *Mr* [18]. *Hc* and *Mr* results are reported in Table 1.

Table 1. Coercivity (*Hc*) and remanent magnetization per gram of oxide (*Mr*) for different analized samples. Results where estimated fitting *M(H)* for low $|H|$ values.

PAA	Sample	Hc (Oe)	Mr (emu/g OFe)
PAA 1800	4.9 mmol/ gOFe	0.12	0.012
	7.5 mmol/ gOFe	0.07	0.003
PAA 5000	10.5 mmol/ gOFe	0.09	0.015
	12.3 mmol/ gOFe	0.08	0.017

Samples have shown intense nonlinear magnetic response, together with low coercivity and low remanent magnetization. Thus, they have shown superparamagnetic response.

According to Chantrel *et al.* [31], *i*t was assumed that nanoparticles are made of single (magnetic) domain crystals whose dipole moment is proportional to their volume. Size distribution was modeled by a log-normal distribution: the volume fraction of nanoparticles with diameter between *D* and *D+dD* is *F(D) dD*,

$$\mathrm{F(D)} = \frac{1}{\mathrm{D\ s_l}\sqrt{2\pi}} \exp\left(-\left[\ln\left(\frac{\mathrm{D}}{\mathrm{D_l}}\right)\right]^2 / 2\ \mathrm{s_l^2}\right) \qquad \text{[Equation 3]}$$

where D_l is the most probable particle diameter and s_l is a (unitless) measure of particle size dispersion (particle size dispersion is $D_l\ s_l$). Interactions among particles have been neglected. The contribution to magnetization from solvent, PAA and linear terms in oxide is modeled through a linear term, *KL*. Under these assumptions it is straightforward to show that Magnetization per gram of oxide, M, as a function of applied magnetic field, H, is described by:

$$\mathrm{M} = \mathrm{M_s} \int_0^\infty \mathrm{L(Ms\ \rho\ V\ H\ /\ kb\ T)\ F(D)\ dD} + \mathrm{K_L\ H} \qquad \text{[Equation 4]}$$

where *L(x)* is the Langevin function, *L(x)=coth(x)-1/x*; *Ms* is the saturation magnetization per gram of oxide; ρ is oxide density; $V = \pi\ D^3/6$ is particle volume; *kb* is Boltzmann constant and *T* is the absolute temperature.

First the linear contribution, *KL*, was substracted. It was estimated from *M(H)* for great values of $|H|$. There, it was considered that both linear terms and also the asymptotic nonlinear terms were present.

Following the procedure proposed by Chantrell [31], for each value of *Ms* it was found approximate values of D_l and s_l. Equation 4 was also employed for describing the data, with D_l, s_l, and M_s as fitting parameters. In order to do so, a computer code was programed, based on Levengand-Marquandt algorithm, which fits the data. The code works as follows. For a given value of D_l , s_l., and *Ms*, M(H) curve is calculated through eq. 4 and compared to experimental data. The distance among theoretical and experimental values of M(H) is calculated through *Err*, defined below. Numerical derivatives of *Err* to D_l , s_l., and *Ms* are also computed. With that information, better estimates of D_l , s_l., and *Ms* chosen. Process is repeated until D_l , s_l., and *Ms* values stop evolving. The code was compiled in gfortran (gcc version 7.1.0) and ran on an i7 computer under Linux (CentOSPlus distribution for x86_64 arhitecture).

Best values for D_l, s_l, and M_s are shown in Table 2. From this values, we are able to report <*D*> and σ, *i.e* the average particle diameter and its standard deviation, respectively. The sum of the squares of the residuals, *Err*, was also calculated:

$$\text{Err} = \sum_i [\,M_o(H_i) - M_e(H_i)]^2 / [\,M_c]^2 \qquad \text{[Equation 5]}$$

where *Hi* are the values for which we measure *M,* M_o is the measured value, M_e is the fitted one, and M_c is a typical magnetization value, considered so that *Err* is unitless. Here it was chosen M_c = 1 emu/g. Clearly, this definition of *Err* grows with the number of data points. Thus, *Err* is only meaningful if it is used for comparing different fits of the same data. As expected, 3-variable-fit gives better results (compared through *Err*) than single-variable fit. It was also checked that reported values are robust, *i.e*. they are insensitive of the initial guesses of D_l, s_l, and M_s .

Table 2. Parameters obtained from our 3-variable-fit under log-normal size distribution.

	Sample	Ms (emu/g OFe)	Dl (nm)	σ l	<D> (nm)	σ (nm)
PAA 1800	4.9 mmol/ gOFe	38.8	10.5	0.50	11.9	6.3
	7.5 mmol/ gOFe	39.3	6.19	0.58	7.3	4.7
PAA 5000	10.5 mmol/ gOFe	75.3	7.75	0.52	8.9	5.0
	12.3 mmol/ gOFe	58.7	9.74	0.49	11	5.7

Magnetic particle size histograms, obtained from TEM images, are shown in Figure 11. They do not seem to represent a log-normal distribution. Then, it was studied how the values of *Ms,* <*D*> and σ depend on the shape of particle size distribution. For this, a 3-variable-fit for a linear distribution of particle sizes was performed (as described in [32]). A Normal distribution of particle sizes, and single valued particle sizes (i.e. σ =0) were also employed. Representative results obtained are shown in Table 3.

Table 3. Parameters obtained by considering different particle size distributions.

	Log-Normal	Linear	Normal	Single Diameter
Ms (emu/g OFe)	58.7	58.1	63.7	55.2

<D> (nm)	11.0	11.3	9.7	10.5
σ (nm)	5.7	5.7	5.0	0
Err	$3.1\ 10^{-5}$	$3.3\ 10^{-3}$	$7.2\ 10^{-5}$	$4.0\ 10^{-3}$

For a linear distribution of particle sizes (instead of log-normal), it was found similar values of *Ms, <D>* and *σ*, although *Err* was greater. Roughly grater values of *Ms* and smaller values of *<D>* and *σ* (and similar *Err*) are found if a Normal distribution of sizes is assumed. Finally, if single valued dipoles are assumed, similar values of *Ms* and *<D>* are obtained, but with higher *Err* (worse fit). Similar results hold for all our samples. The data along with the fit was plotted, as in Fig. 12, for all studied particle size distribution shapes (not shown). As expected from *Err*, Log-Normal and Normal size distributions show much better fits. It can be concluded that choosing the right shape of particle distribution is not central for getting estimates of *Ms, <D>* and *σ*, while better fits are found with Normal and Log-Normal particle size distributions.

Saturation magnetization per gram of oxide, *Ms*, lies between 38.8 and 75.3 emu/g. Values in literature yield similar broad results (from about 20 [33] to 81.6 emu/g [34]). Possible explanations for the broad range of values for *Ms* include the partial formation of Maghemite instead of Magnetite in part of the samples, disorder and surface effects. Saturation Magnetization for bulk magnetite is 90-95 emu/g, while it is about 76 emu/g for bulk Maghemite [35,36]. Thus, partial formation of Maghemite cannot completely explain the obtained results. An explanation involving spin canting in the whole volume of some particles, disorder in the whole particle and surface effects may be better suited [37].

From magnetization results, average particle sizes between 6.2 and 11.9 nm were estimated. They are similar to values reported elsewhere under different procedures (ranging from 3 to 50 nm) [33]. The size derived from magnetization experiments are comparable with those results obtained from both XRD and TEM images. This suggests that the single domain picture holds for our samples.

4. Conclusions

A set of PAA-coated iron oxide MNPs were successfully prepared through coprecipitation method. In addition to the influence of PAA's contents, the main studied variable was the

influence of PAA's Mw on the final properties of MNPs. Thus, two low molecular weights were employed, 1800 and 5000, in three different reactor feeds. The presence of a mixture of iron oxides in the MNPs mainly corresponding to PAA-coated Fe_3O_4 and Fe_2O_3 was confirmed by XRD.

According to TGA results, higher PAA's Mw leads to a higher MNPs PAA content for each reactor feed. Even though this fact is already reported, here we found that it can also be observed by employing two near low molecular weights. PAA's contents have an influence towards particle size and hydrodynamic diameter of the MNPs and also on their size distribution: higher PAA's quantities lead to smaller sizes and narrower size distributions. The z potential values appear to be more dependent on PAA content than on their PAA's Mw.

Chemical interactions between PAA and iron oxides through symmetrical bidentate bridging were confirmed by FTIR measurements.

Magnetization analysis shows that all samples present superparamagnetic response, with very low coercivity and remanent magnetization at room temperature. Magnetic response was modeled assuming a distribution of magnetic particle sizes. Log-Normal and Normal size distributions gave excellent results. Magnetic diameter was estimated, ranging from 7.3 to 11.9 nm. These values are comparable with results from TEM image analysis, and thus, support the single crystal image. A broad distribution of magnetic particle sizes was found. Saturation magnetization per gram of oxide was lower than results for bulk Magnetite. This may be explained through disorder of the magnetic moments inside the particles.

5. Acknowledgements

This study was supported by CONICET (National Scientific and Technical Research Council), ANPCyT (National Agency of Scientific and Technology Promotion), UNMdP (National University of Mar del Plata) and Bunge & Born Foundation (L. Sanchez, Postdoctoral Research Grant). Authors would like to thank M. L. Arciniegas Vaca for magnetization measurements.

6. Bibliography

[1] A.M. Abu-dief, S.M. Abdel-fatah, Development and functionalization of magnetic nanoparticles as powerful and green catalysts for organic synthesis, Beni-Suef Univ. J. Basic Appl. Sci. In Press (2017). doi:10.1016/j.bjbas.2017.05.008.

[2] P.S. Williams, F. Carpino, M. Zborowski, Magnetic Nanoparticle Drug Carriers and Their Study by Quadrupole Magnetic Field-Flow Fractionation, Mol. Pharm. 6 (2009) 1290–1306.

[3] C. Felton, A. Karmakar, Y. Gartia, P. Ramidi, A.S. Biris, A. Ghosh, Magnetic nanoparticles as contrast agents in biomedical imaging: recent advances in iron- and manganese-based magnetic nanoparticles., Drug Metab. Rev. 46 (2014) 142–154. doi:10.3109/03602532.2013.876429.

[4] P. Nicolas, V. Lasalle, M.L. Ferreira, Development of a magnetic biocatalyst useful for the synthesis of ethyloleate, Bioprocess Biosyst. Eng. 37 (2014) 585–591. doi:10.1007/s00449-013-1010-7.

[5] M.F. Horst, D.F. Coral, M.B. Fernández, V. Raap, M. Alvarez, V. Lassalle, Hybrid nanomaterials based on gum Arabic and magnetite for hyperthermia treatments, Mater. Sci. Eng. C. 74 (2017) 443–450. doi:10.1016/j.msec.2016.12.035.

[6] A.S. Teja, P. Koh, Synthesis , properties , and applications of magnetic iron oxide nanoparticles, Prog. Cryst. Growth Charact. Mater. 55 (2009) 22–45. doi:10.1016/j.pcrysgrow.2008.08.003.

[7] H. Shokrollahi, A review of the magnetic properties, synthesis methods and applications of maghemite, J. Magn. Magn. Mater. 426 (2017) 74–81. doi:10.1016/j.jmmm.2016.11.033.

[8] M. Răcuciu, Synthesis protocol influence on aqueous magnetic fluid properties, Curr. Appl. Phys. 9 (2009) 1062–1066. doi:10.1016/j.cap.2008.12.003.

[9] E. Tombácz, I.Y. Tóth, D. Nesztor, E. Illés, A. Hajdú, M. Szekeres, L. Vékás, Adsorption of organic acids on magnetite nanoparticles , pH-dependent colloidal stability and salt tolerance, Colloids Surfaces A Physicochem. Eng. Asp. 435 (2013) 91–96. doi:10.1016/j.colsurfa.2013.01.023.

[10] E. Tombácz, M. Szekeres, A. Hajdú, I.Y. Tóth, R. Andrea, D. Nesztor, E. Illés, I. Zupkó, L.

Vékás, Colloidal stability of carboxylated iron oxide nanomagnets for biomedical use, Period. Polytech. Chem. Eng. 58 (2014) 3–10. doi:10.3311/PPch.7285.

[11] S. Liufu, H. Xiao, Y. Li, Adsorption of poly (acrylic acid) onto the surface of titanium dioxide and the colloidal stability of aqueous suspension, J. Colloid Interface Sci. 281 (2005) 155–163. doi:10.1016/j.jcis.2004.08.075.

[12] S. Chibowski, M. Wis, Study of electrokinetic properties and structure of adsorbed layers of polyacrylic acid and polyacrylamide at Fe2O3 – polymer solution interface, Colloids Surfaces A Physicochem. Eng. Asp. 208 (2002) 131–145.

[13] L.A. Puentes-Vara, K.M. Gregorio-Jauregui, A.M. Bolarín, M.E. Navarro-Clemente, H.J. Dorantes, M. Corea, Effects of surfactant and polymerization method on the synthesis of magnetic colloidal polymeric nanoparticles, J. Nanoparticle Res. 18 (2016) 1–18. doi:10.1007/s11051-016-3524-9.

[14] M. Rutnakornpituk, N. Puangsin, P. Theamdee, B. Rutnakornpituk, U. Wichai, Poly(acrylic acid)-grafted magnetic nanoparticle for conjugation with folic acid, Polymer (Guildf). 52 (2011) 987–995. doi:10.1016/j.polymer.2010.12.059.

[15] P. Padwal, R. Bandyopadhyaya, S. Mehra, Polyacrylic Acid-Coated Iron Oxide Nanoparticles for Targeting Drug Resistance in Mycobacteria, Langmuir. 30 (2014) 15266–15276. doi:10.1021/la503808d.

[16] Y. Xu, L. Zhuang, H. Lin, H. Shen, J.W. Li, Preparation and characterization of polyacrylic acid coated magnetite nanoparticles functionalized with amino acids, Thin Solid Films. 544 (2013) 368–373. doi:10.1016/j.tsf.2013.02.097.

[17] I.S. Smolkova, N.E. Kazantseva, H. Parmar, V. Babayan, P. Smolka, P. Saha, Correlation between coprecipitation reaction course and magneto-structural properties of iron oxide nanoparticles, Mater. Chem. Phys. 155 (2015) 178–190. doi:10.1016/j.matchemphys.2015.02.022.

[18] C.L. Lin, C.F. Lee, W.Y. Chiu, Preparation and properties of poly(acrylic acid) oligomer stabilized superparamagnetic ferrofluid, J. Colloid Interface Sci. 291 (2005) 411–420. doi:10.1016/j.jcis.2005.05.023.

[19] C.A. Fyfe, M.S. McKinnon, Investigation of the thermal degradation of poly(acrylic acid) and poly(methacrylic acid) by high-resolution carbon-13 CP/MAS NMR spectroscopy,

Macromolecules. 19 (1986) 1909–1912. doi:10.1021/ma00161a021.

[20] H.G. Schild, Thermal Degradation of Poly (methacrylic acid): Further Studies Applying TGA/ FTlR, J. Polym. Sci. Part A Polym. Chem. 31 (1993) 2403–2405.

[21] M.A.C. Stuart, Adsorbed Polymers in Colloidal Systems: from Statics to Dynamics, Polym. J. 23 (1991) 669–682.

[22] S. Chibowski, E.O. Mazur, J. Patkowski, Influence of the ionic strength on the adsorption properties of the system dispersed aluminium oxide – polyacrylic acid, Mater. Chem. Phys. 93 (2005) 262–271. doi:10.1016/j.matchemphys.2005.02.038.

[23] S. Chibowski, M. Paszkiewicz, Influence of the Molecular Weight of Polyethylene Glycol and Polyethylene Oxide on the Adsorption and Electrochemical Properties of the Titania/Electrolyte Solution Interface, Adsorpt. Sci. Technol. 17 (1999) 845–855.

[24] K. Vermohlen, H. Lewandowski, H. Narres, E. Koglin, Adsorption of polyacrylic acid on aluminium oxide : DRIFT spectroscopy and ab initio calculations, Colloids Surfaces A Physicochem. Eng. Asp. 170 (2000) 181–189.

[25] A. Hajdú, M. Szekeres, I.Y. Tóth, R.A. Bauer, J. Mihály, I. Zupkó, E. Tombácz, Enhanced stability of polyacrylate-coated magnetite nanoparticles in biorelevant media, Colloids Surfaces B Biointerfaces. 94 (2012) 242–249. doi:10.1016/j.colsurfb.2012.01.042.

[26] S. Bruni, F. Cariati, M. Casu, A. Lai, A. Musinu, G. Piccaluga, S. Solinas, IR and NMR study of nanoparticle-support interactions in a Fe2O3-SiO2 nanocomposite prepared by a Sol-gel method, Nanostructured Mater. 11 (1999) 573–586. doi:10.1016/S0965-9773(99)00335-9.

[27] V.K. Gupta, A. Nayak, Cadmium removal and recovery from aqueous solutions by novel adsorbents prepared from orange peel and Fe 2O 3 nanoparticles, Chem. Eng. J. 180 (2012) 81–90. doi:10.1016/j.cej.2011.11.006.

[28] F. Jones, J.B. Farrow, W. van Bronswijk, An Infrared Study of a Polyacrylate Flocculant Adsorbed on Hematite, Langmuir. 14 (1998) 6512–6517.

[29] R. Omidirad, F. Rajabi Hosseinpour, B. Farahani, Preparation and in vitro drug delivery response of doxorubicin loaded PAA coated magnetite nanoparticles, J. Serbian Chem. Soc. 78 (2013) 1609–1616. doi:10.2298/JSC121225041O.

[30] K.Y. Yoon, C. Kotsmar, D.R. Ingram, C. Huh, S.L. Bryant, T.E. Milner, K.P. Johnston, Stabilization of Superparamagnetic Iron Oxide Nanoclusters in Concentrated Brine with Cross-Linked Polymer Shells, Langmuir. 27 (2011) 10962–10969.

[31] R. Chantrell, J. Popplewell, S. Charles, Measurements of particle size distribution parameters in ferrofluids, IEEE Trans. Magn. 14 (1978) 975–977. doi:10.1109/TMAG.1978.1059918.

[32] S.H. Mahmood, Magnetic anisotropy in fine magnetic particles, J. Magn. Magn. Mater. 118 (1993) 359–364. doi:10.1016/0304-8853(93)90439-9.

[33] S. Laurent, D. Forge, M. Port, A. Roch, C. Robic, L. V Elst, R.N. Muller, Magnetic Iron Oxide Nanoparticles: Synthesis, Stabilization, Vectorization, Physicochemical Characterizations, and Biological Applications, Chem. Rev. 108 (2008) 2064–2110. doi:Doi 10.1021/Cr900197g.

[34] Y.-Y. Xu, M. Zhou, H.-J. Geng, J.-J. Hao, Q.-Q. Ou, S.-D. Qi, H.-L. Chen, X.-G. Chen, A simplified method for synthesis of Fe3O4@PAA nanoparticles and its application for the removal of basic dyes, Appl. Surf. Sci. 258 (2012) 3897–3902. doi:10.1016/j.apsusc.2011.12.054.

[35] J. Smit, H.P.J. Wijn, Ferrites. Physical properties of ferrimagnetic oxides in relation to their technical applications., 1959.

[36] E. Lima, E. De Biasi, M.V. Mansilla, M.E. Saleta, F. Effenberg, L.M. Rossi, R. Cohen, H.R. Rechenberg, R.D. Zysler, Surface effects in the magnetic properties of crystalline 3 nm ferrite nanoparticles chemically synthesized, J. Appl. Phys. 108 (2010) 103919 1-10. doi:10.1063/1.3514585.

[37] M.P. Morales, S. Veintemillas-Verdaguer, M.I. Montero, C.J. Serna, A. Roig, L. Casas, B. Martinez, F. Sandiumenge, Surface and Internal Spin Canting in gamma -Fe2O3 Nanoparticles, Chem. Mater. 11 (1999) 3058–3064.